UNITED NATIONS UNIVERSITY
UNU-GTP
Geothermal Training Programme

Orkustofnun, Grensasvegur 9,
IS-108 Reykjavik, Iceland

Reports 2017
Number 9

PILOT COGENERATION PLANT FOR PUGA GEOTHERMAL FIELD: PROVIDING CLEAN ENERGY SOLUTION TO A NOMADIC RESIDENTIAL SCHOOL IN PUGA, INDIA

Kunzes Dolma
Ladakh Renewable Energy Development Agency (LREDA),
Ladakh Autonomous Hill Development Council (LAHDC),
Block 2, Mini Sect., LAHDC Complex, Leh-194101,
Jammu and Kashmir,
INDIA
kdolma999@gmail.com

ABSTRACT

The paper discusses the design of a pilot Binary power plant to electrify the Nomadic Residential School (NRS) in Puga, India. With the existing well and surface temperature of 80°C it is possible to generate more than 60 kW of electricity which is more than enough to electrify the school building continuously for 24 hours per day. Consideration were also made to use a screw expander instead of a turbine to reduce the cost of the project. The demand on the design accuracy for a turbine increases rapidly when the size becomes smaller, whereas the same demands do not change much for a screw expander. The design of a heating system for the school using the available geothermal fluid is also discussed. Calculation was made for heat load of the building without insulation (present scenario) and with building insulation. The results show that for long term energy savings it would be good to insulate the building which will reduce the heat load by more than half of the present heat load. The main objective is to provide a clean and sustainable energy solution with a comfortable indoor temperature of 20°C, even when outside temperature can go below -20°C.

1. INTRODUCTION

The scope of this report is to explore how the existing flowing geothermal well in Puga can be used without further drilling to generate electricity which will be enough to electrify and run the direct heating system for the Nomadic Residential School. At present, the boarding school is heated using wood or kerosene. For electricity there is a 10 kVA standalone generator which supplies electricity to the boarding school from 6pm to 11pm. There are three villages nearby namely Sumdo TR, Sumdo and Korzok. Sumdo and Sumdo TR have no access to electricity at all. The electricity requirement of Korzok is fulfilled by a diesel generator of 82.5 kVA/66 kW which only operates from 6 to 11 pm (District Statistical and Evaluation Office, 2015). With the construction of the new administration block in Puga there will be more demand for electricity which can be met with this plant. This utilisation of this resource is important keeping in view the fact that the diesel required to electrify these areas must be transported from other states of India in tankers which adds to the increasing carbon dioxide emissions.

The exploitation of this field is very important at a stage when the whole world is fighting to decrease CO_2 emissions and to fulfil India's goal in combating human induced climate change. Furthermore, it is important in achieving the United Nations' Sustainable Development Goals. In particular Goal 7 which aims to ensure access to affordable, reliable, sustainable and modern energy for all. The Goals were set out by the UN to reduce poverty and push development in the world (United Nations, 2015).

2. FIELD INFORMATION

FIGURE 1: Geothermal provinces of India (Craig et al, 2013)

Puga, shown in Figure 1, is a valley located at 4550 m elevation above sea level with a latitude of 33˚13' N and longitude 78˚18' E, at the junction of the Indian and Tibetan plates along the Indus Suture Zone and has geothermal manifestations in the form of hot springs, mud pools, sulphur and borax deposits covering an area of 15 square kilometres. Puga geothermal field is bounded by faults and its reservoir rocks consist of granite, gneiss and schist. Geophysical surveys show a low resistivity zone below the Puga field (Singh et al., 1983; Harinarayana et al., 2004; Azeez and Harinarayana, 2007). Methodical and comprehensive evaluations of the field begun in 1973. Out of the 34 wells that were drilled, 17 wells had mixed steam and water blow-outs. Some wells show discharge of more than 120°C. Thermal studies show temperatures of more than 220°C at 2200 m depth while chemical thermometry shows a reservoir temperature of 250°C and reservoir modelling shows temperatures of up to 160°C at 450 m depth. The geothermal fluid has high concentrations of lithium, rubidium and caesium, indicating that the heat source for Puga is a magmatic source. Observations indicate that the Puga field could sustain a 20 MW_e power plant (Craig et al, 2013).

The specifications of the Puga field are given in Table 1:

TABLE 1: Specifications of the Puga geothermal field

Particulars	Values
Temperature of fluid	80°C surface temperature
Estimated reservoir temperature at 2000 m depth	Over 200°C
Area of the geothermal field	5 km^2
Number of wells drilled	34
Cumulative Discharge	30 l/s
Estimated potential of the field	Over 20 MWe

2.1 Geothermal water quality

A speciation calculation was made using the WATCH computer program for the geothermal water at 85°C, assuming pH = 8.2, suggests that the water is exactly at the saturation limit with respect to calcite at this temperature. Therefore, there should be no risk of calcite scaling when the water is cooled during utilisation due to the higher solubility of calcite with decreasing temperature (Pers. Comm., Finnbogi Óskarsson, Geochemist, ISOR, September 2017).

On the other hand, some minor precipitation of amorphous silica may occur upon cooling as the silica concentration of the water is rather high (207 mg/L) according to Shanker et al. (2000). However, the silica concentrations reported by Craig et al. (2013) are rather lower (120-165 mg/L) and should not cause significant precipitation of amorphous silica. The report of the test can be seen in Appendix 1. The geothermal water does not have a pleasant smell and is not likely to be used as tap water.

3. MARKET STUDY FOR HEAT AND ELECTRICITY

Puga is the headquarters of the Rupsho Administrative Region and there are plans to construct several buildings such as a medical centre, the administrative building of the block and staff quarters adding to the existing NRS building. All these will be within 2 km of the geothermal field. Within 5 km of the field there is the Sumdho Tibetan Refugee area with 65 households, a primary school, staff quarters for 15 staff and community hall. Sumdho village has 16 households, a community centre, a medical sub centre, Anganwadi (playschool) and staff quarters. Korzok village with 253 households is a major tourist attraction village because of the Tsomoriri Lake. Figure 2 shows the various market areas around the Puga geothermal field.

FIGURE 2: Location of Puga and the nearby villages

4. WEATHER AND AMBIENT AIR TEMPERATURE

The minimum temperature in the region is around -25 °C and maximum is 25°C (Pers. Comm., Dorjey Wangchuk, Engineer Incharge, Indian Institute of Astrophysics, Leh, August 2017). Figure 3 shows the maximum and minimum temperature for the period 2002 to 2011.

More detailed weather data for the creation of duration curves in Chapter 8.1 was taken from the "International Weather for Energy Calculations" (ASHRAE, 2017) for Shiquanhe, main town of Ngari district in China. This was the closest location available and is at the same altitude. The monthly averages in that data set agree fairly well with the Changthang data, so it was concluded that it could be used to represent the weather in Puga.

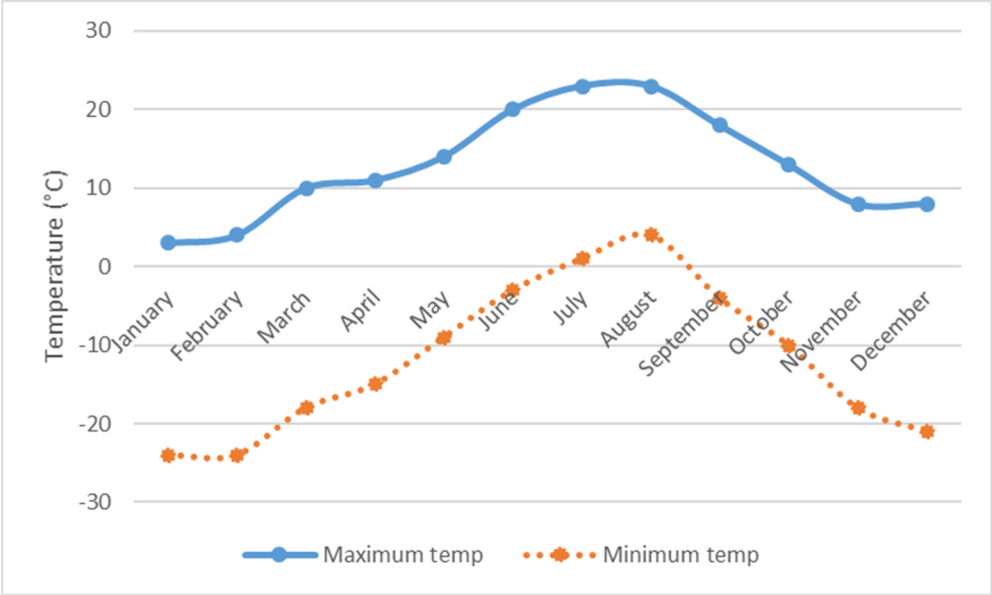

FIGURE 3: Temperature for Changthang

5. THE PROPOSED CO-GENERATION SYSTEM

The purpose was to design cogeneration of electricity and heating for the NRS from the available geothermal fluid (Figure 4). The present expected flow of 12 kg/s would be sufficient to support the ORC plant and the school heating system in parallel. The available fluid will have around 84°C temperature at the source. The main consideration is that the power plant should be able to start without having any electricity available.

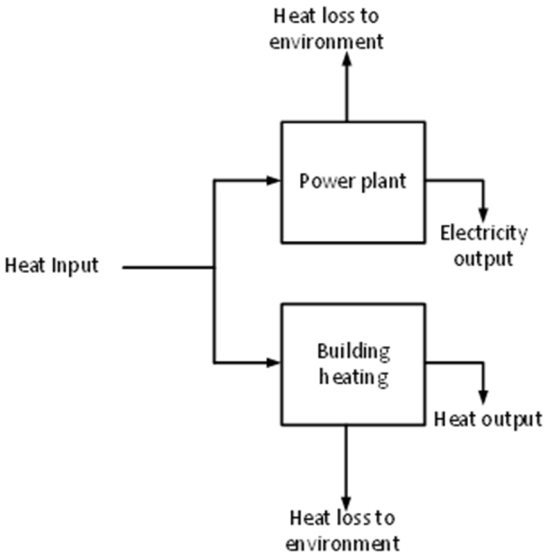

FIGURE 4: Block Diagram for the co-generation

6. POWER PLANT

6.1 Geothermal power plants and cogeneration

There are three basic systems typically in use in the world today to convert geothermal energy into electricity (Elíasson et al., 2008) as shown in Table 2:

TABLE 2: Systems to convert geothermal energy into electricity

System	Resource temperature range
Flashed steam/ dry steam condensing system	230 - 320°C
Flashed steam back pressure system	200 - 320°C
Binary or twin-fluid system	120 - 190°C

6.2 The proposed plant

There is no electricity grid available in Puga, except for the standalone diesel generator engine of 10 kVA. The diesel generator would most likely be used as a reserve in the future. The ORC power plant thus has to be able to start without any power present.

In case the pressure from the wells is not sufficient to get enough fluid running through the ORC heat exchangers to start the plant, a "tank" design must be used, where the low pressure natural flow is collected into a tank (Figure 5). The heat exchangers with the working fluid at the tube side are then dipped into the pool. The disadvantage of this design is that oxygen from air will be absorbed in the geothermal water and cause corrosion, unless appropriate corrosion resistant material is used for the heat exchangers. Since water is scarce in the area, air cooled condensers will be used to cool the working fluid coming out of the turbine.

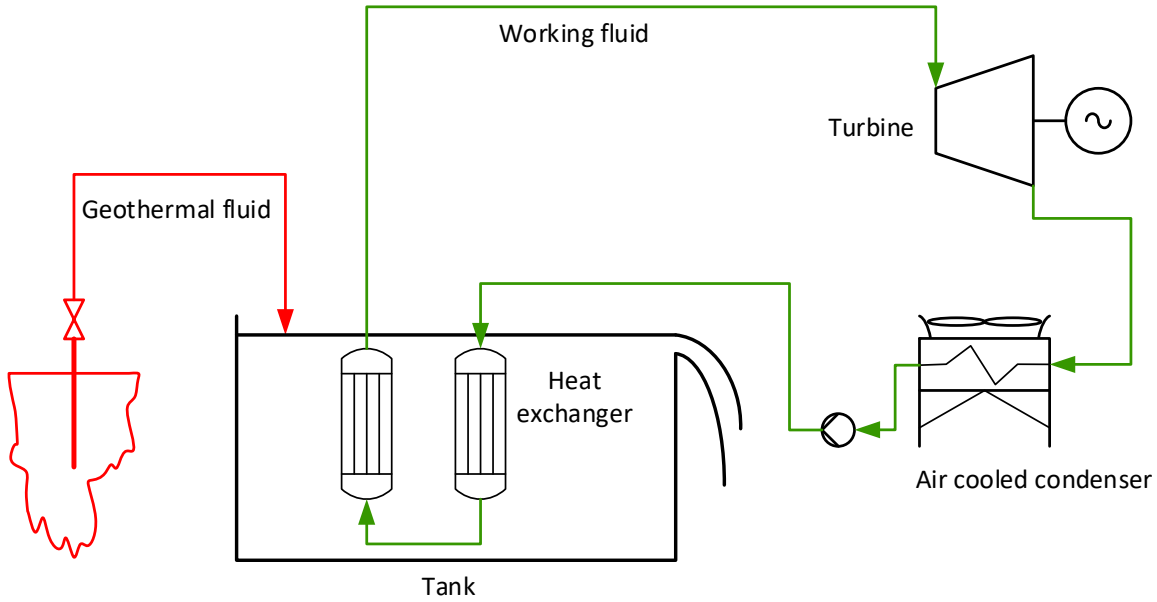

FIGURE 5: Diagram of a power plant with a "tank"

It is likely that the wells would have sufficient pressure to force some fluid through the heat exchangers, so that the plant can be started without the use of a pump. The selected power plant is thus a conventional ORC with shell and tube heat exchanger.

6.3 ORC plant design

A traditional shell and tube heat exchanger requiring fluid pressure of around 1.5 or 2 bars at the inlet of the heat exchangers was assumed here (Figure 6). The geothermal fluid is on the inside of the tubes, and the working fluid on the shell side. The inside of the tubes can be mechanically cleaned, if there is any dirt or precipitation present from the geothermal fluid. The shell can be manufactured from inexpensive black steel as the working fluid is not corrosive. The tubes will most likely have to be made out of corrosion-resistant steel as the geothermal fluid is very likely to be corrosive for black steel.

The ORC working fluid is in a closed circuit in the plant. The fluid is condensed into liquid phase in the air-cooled condenser, and enters the circulation pump as liquid at a low temperature and low pressure.

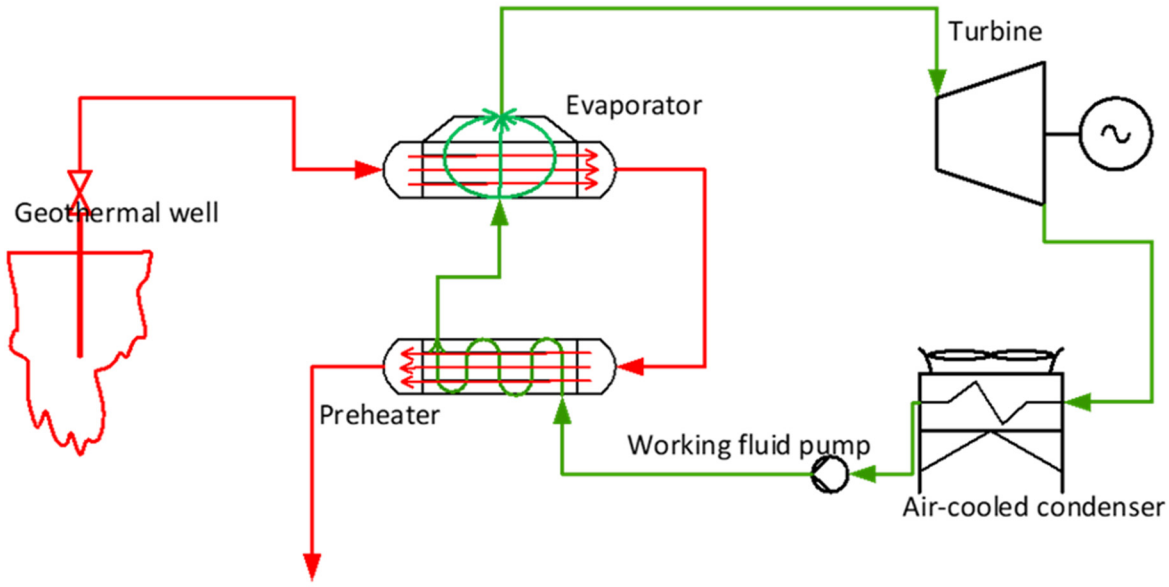

FIGURE 6: Diagram of the shell and tube heat exchanger plant

The circulation pump increases the working fluid pressure up to the vaporizer pressure which has been selected for the plant. The liquid working fluid is now at a high pressure and enters the preheater, where the fluid is heated by the geothermal fluid up to a temperature just below the boiling temperature of the selected working fluid pressure. After that the working fluid enters the vaporizer, where the fluid is heated further to the bubble point, where boiling starts.

The boiling of the working fluid continues in the vaporizer at a constant temperature, where an increasing mass fraction of the working fluid changes the phase from liquid to vapour. Heat for the vaporization process is taken from the geothermal fluid on the tube side of the vaporizer. Finally, there is no liquid present anymore, and all the working fluid has been transformed into vapour. The vapour becomes ever so slightly superheated through contact with the hot geothermal fluid tubes above the liquid surface in the vaporizer.

The high-pressure vapour now enters the turbine or screw expander, whichever has been selected. There, the working fluid vapour expands down to the condenser pressure and performs work, which is transferred to the generator as shaft power. The spent vapour from the turbine is now at low pressure and is led to the air-cooled condenser, where it will condense again into liquid.

6.4 Expander or turbine?

A screw expander is a displacement expander, and is thermodynamically like a piston expander. It is volumetric. The volumetric expansion ratio is determined by the internal geometry of the expander and cannot be changed. There is no conversion of enthalpy into kinetic energy as in the turbine. This has both benefits and disadvantages. The screw expander is not sensitive to droplets or dirt in the incoming vapour, as there are no extremely high velocities in the expander, opposed to the turbine where the maximum vapour velocity is at least the sonic velocity of the vapour. The mechanical design of the expander is not as advanced as the turbine due to the same reason. The turbine will have a high rotational speed, resulting in high centrifugal forces, demanding expensive material and a very thorough analysis of stress and vibration. The price of a screw expander is considerably less than that of a turbine due to the same reason. The demand on the design accuracy for a turbine increases rapidly when the size becomes smaller, whereas the same demands do not change much for a screw expander. A smaller

screw expander may even be easier to design and build than a large one. This results in that it is not likely that a turbine can become competitive at all for the sizes expected for this project.

The disadvantage of the screw expander compared to the turbine is that the isentropic efficiency is lower, typically around 70% where a turbine may have around 80% efficiency. Screw expanders have been applied successfully in geothermal power generation in Yangbajing, China. They have extremely good characteristics like anti-contamination, self-cleaning, simple system structure, few spare parts, convenient maintenance, high equipment reliability and long service time (Yue-feng et al., 2015).

6.5 Analysis

A process flow diagram for the plant is shown in Figure 7. The thermodynamic stations for the working fluid are numbered 1 through 8, the stations for the geothermal source fluid as s1 through s5 and the cooling air as c1 through c3.

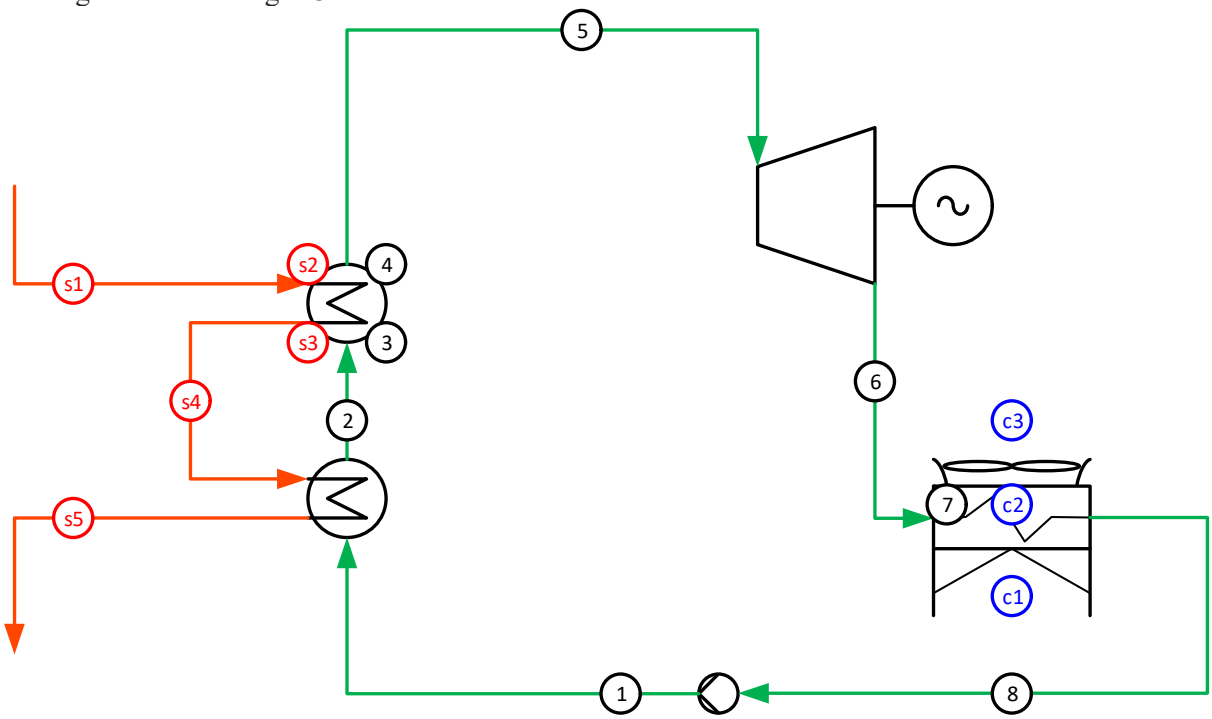

FIGURE 7: Process flow diagram for the power plant

The thermodynamic stations are as follows:

1 Working fluid at the circulation pump outlet.
2 Working fluid at the preheater inlet.
3 Working fluid at the bubble point (creation of first bubble).
4 Working fluid at dew point (evaporation of last liquid droplet).
5 Working fluid at expander entry.
6 Working fluid at condenser entry.
7 Working fluid at condenser dew point (creation of first working fluid droplet).
8 Working fluid at condenser outlet (hot well).

s1 Geothermal source fluid at plant inlet.
s2 Geothermal source fluid at working fluid dew point.
s3 Geothermal source fluid at working fluid bubble point.
s4 Geothermal source fluid at vaporizer outlet.
s5 Geothermal source fluid at plant outlet.

c1 Cooling air at condenser inlet.
c2 Cooling air at condenser working fluid dew point.
c3 Cooling air at condenser outlet.

The temperature-entropy diagram for the cycle is shown in Figure 8. The naming of the thermodynamic stations is the same as in the process flow diagram. The curves for the geothermal source fluid and the cooling air have been added to the diagram, matching the appropriate points for the working fluid.

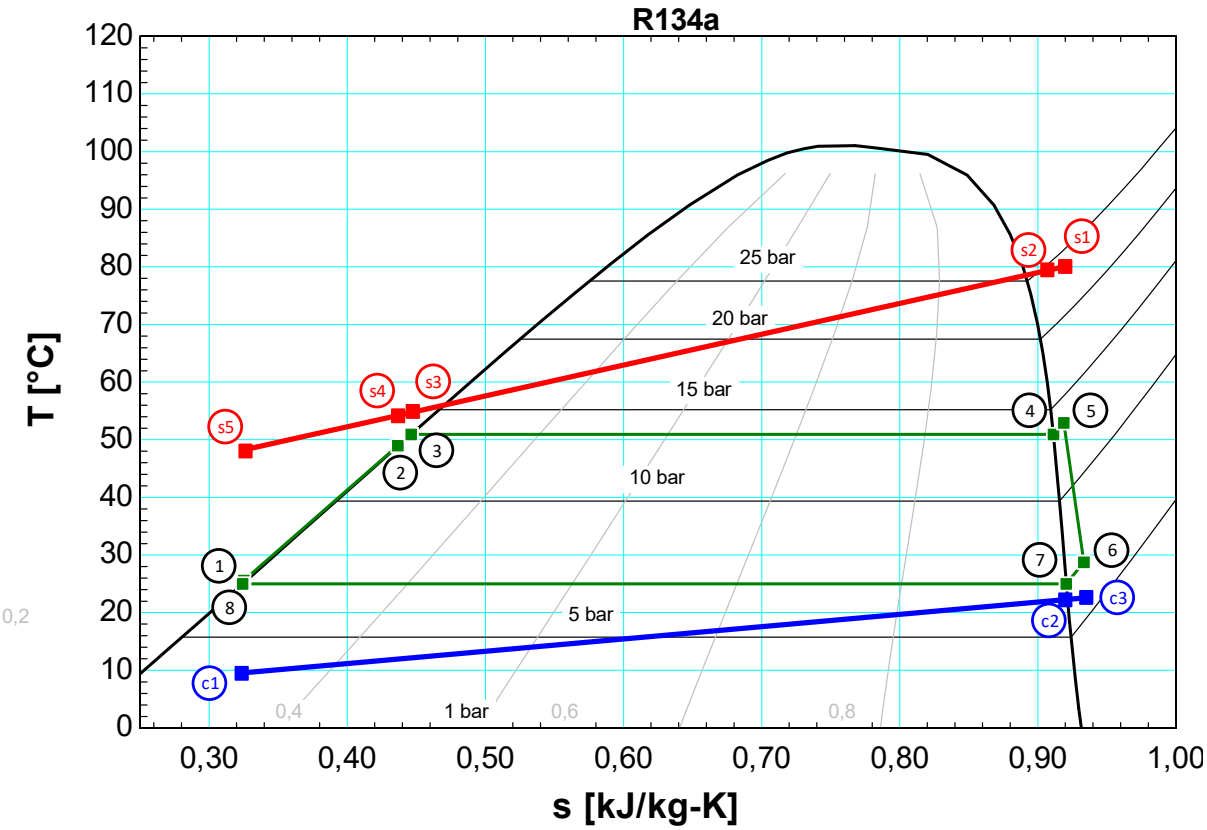

FIGURE 8: T-s (temperature-entropy) diagram for the thermodynamic cycle

The following design parameters have been assumed for the plant:

T_{s1}	= 80°C
$\dot{m}_s$	= 30 l/s
Ps	= 10 bar
T_8	= 25°C
$T_{\text{boiling margin}}$	= 2°C
P_1	= 3 bar
η_{turbine}	= 85%
$T_{\text{pre vap}}$	= 4°C
T_{s5}	= 60°C

where

T_{s1}	= Temperature of source at point s1.
$\dot{m}_s$	= Mass flow rate of geothermal fluid at the wellhead.
P_s	= Pressure of geothermal fluid at point s1.
T_8	= Temperature of the working fluid at point 8, condensation.
P_1	= Pressure at entry of vaporizer, point 1.
$\dot{Q}_{superheat}$	= Heat duty of superheat.

$\dot{Q}_{vap\ pre}$ = Heat duty of preheating within vaporizer.
$\dot{Q}_{cond}$ = Heat duty of condenser.
$\dot{Q}_{cond,condensation}$ = Heat duty in condensation within condenser.
$\dot{Q}_{cond,desuper}$ = Heat duty in desuperheat within condenser.
η_{isen} = Isentropic turbine efficiency.
η_{pump} = Pump isentropic efficiency of turbine.
$T_{pinch\ vap}$ = Vaporizer pinch temperature difference.
T_{s5} = Return temperature of geothermal fluid.
$T_{boiling\ margin}$ = Margin of vaporizer entry temperature to bubble point.

S1 (Figure 9) is the entry point of the source/geothermal fluid where it vaporizes the working fluid and superheats at point s2 in the vaporizer. It then leaves and enters the preheater at point s4 where it heats the working fluid in the preheater and leaves the preheater at point s5 where it is used for the direct heating.

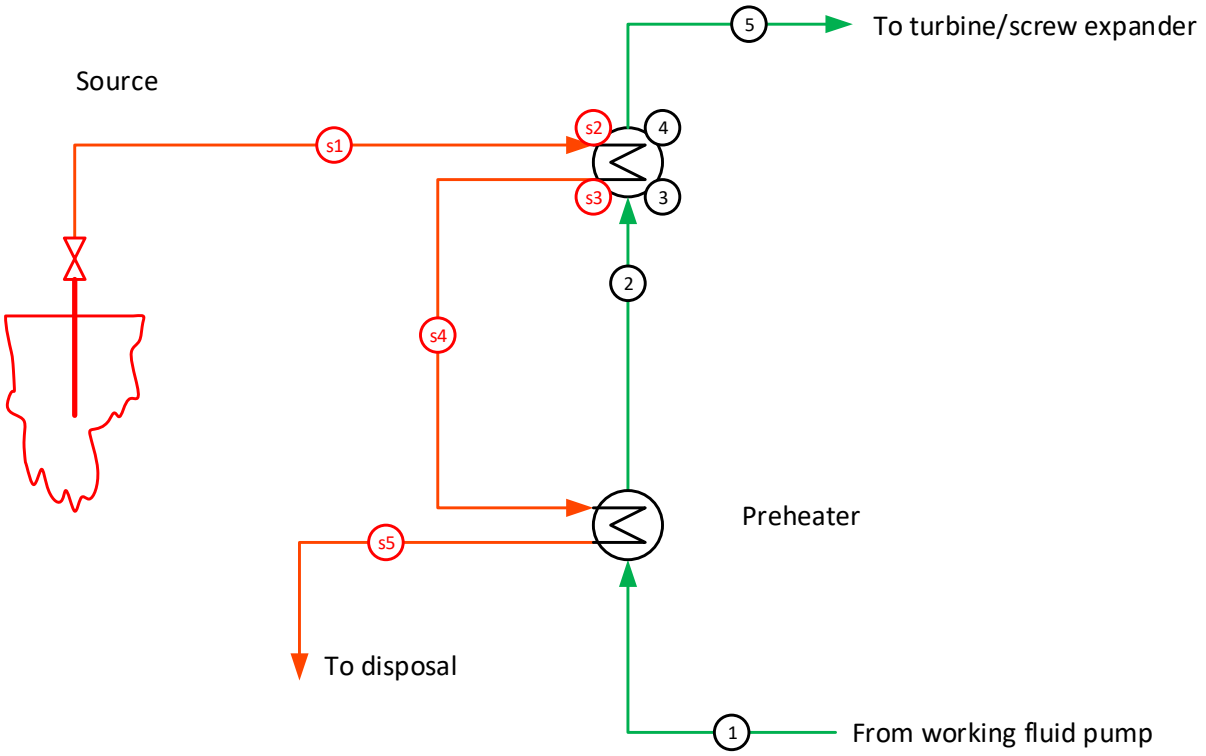

FIGURE 9: Preheater and evaporator

6.5.1 Heat balance at the right hand side

$$\dot{m}_s * (h_{s1} - h_{s3}) = \dot{m}_{wf} * (h_5 - h_4) \quad (1)$$

$\dot{m}_{wf}$ = mass flow rate of working fluid.
h_{s1} = enthalpy of geothermal fluid at point s1.
h_{s3} = enthalpy of geothermal fluid at point s3.
h_5 = enthalpy of working fluid at point 5.
h_4 = enthalpy of working fluid at point 4.

6.5.2 At dew point

Point 2 and point 5 in Figure 9 are the entry and exit points of the working fluid to the vaporiser/super heater. The heat transferred from the geothermal fluid in the super heater has to be equal to the heat added to the working fluid which is given by equation:

$$\dot{Q}_{superheat} = \dot{m}_{wf} * (h_5 - h_4) \quad (2)$$

$$\dot{Q}_{superheat} = \dot{m}_{wf} * (h_{s1} - h_{s2}) \quad (3)$$

6.5.3 At the vaporiser inlet

$$\dot{Q}_{vap\ pre} = \dot{m}_{wf} * (h_3 - h_2) \quad (4)$$

$$\dot{Q}_{dot\ vap\ pre} = \dot{m}_{wf} * (h_{s3} - h_{s4}) \quad (5)$$

6.5.4 Work done by the turbine

Figure 10 shows the thermodynamic process of the turbine. With the assumptions that the process is adiabatic, and neglecting the changes in kinetic and potential energy of the fluid entering and leaving the turbine, the work produced by the turbine per unit mass of steam flowing through it is:

$$W_t = (h_5 - h_6) \quad (6)$$

Maximum possible work is generated if the turbine operates adiabatically and reversibly (at constant entropy/isentropically). Isentropic work is then given by:

$$W_{isen} = (h_5 - h_{6s}) \quad (7)$$

Then the isentropic efficiency of the turbine is the ratio of the actual work done to the isentropic work:

$$\eta_{isen} = (h_5 - h_6)/(h_5 - h_{6s}) \quad (8)$$

Power produced by the turbine will be:

$$\dot{W}_{turbine} = \dot{m}_{wf} \cdot \eta_{isen} \cdot (h_5 - h_{6s}) = \dot{m}_{wf} \cdot (h_5 - h_6) \quad (9)$$

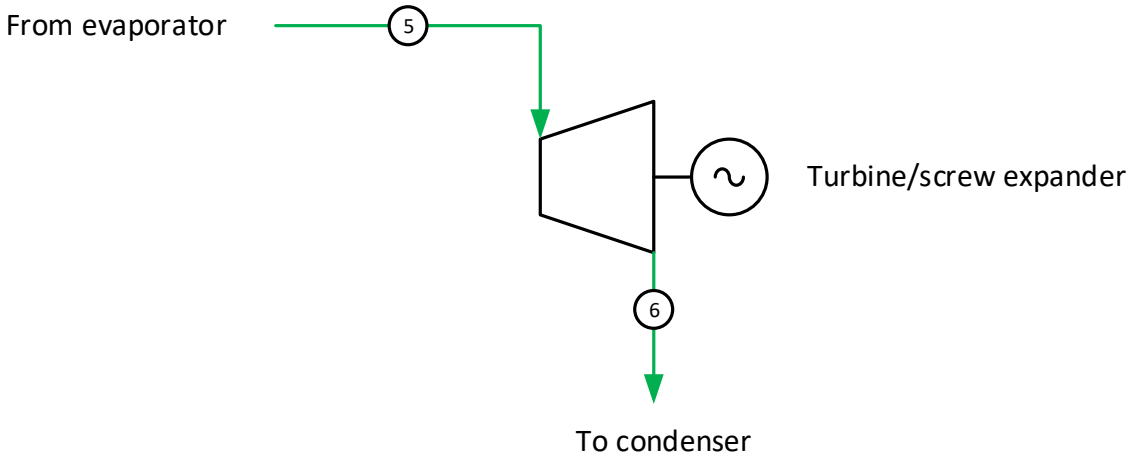

FIGURE 10: Turbine

6.5.5 Pump

Work done by the working fluid pump is shown in Figure 11.

$$\dot{W}_{pump} = \eta_{pump} \cdot \frac{\dot{m}_{wf}}{\rho_{wf}} \cdot (P_1 - P_8) = \dot{m}_{wf} \cdot (h_1 - h_8) \quad (10)$$

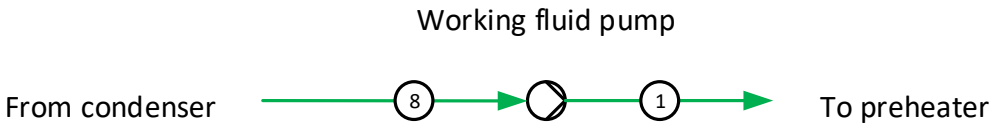

FIGURE 11: Working fluid pump

6.5.6 Net power

Net power generated is given by:

$$W_{net} = \dot{W}_{turbine} - \dot{W}_{pump} \tag{11}$$

6.5.7 Air cooled condenser

Selection of the air cooled condenser (Figure 12) is based on the fact that the area has a scarcity of water. The working fluid enters the condenser at point 6 and is a saturated liquid when it leaves at point 9. The ambient cooling air enters at point c1 and leaves at point c3. Heat rejected by the working fluid to the atmosphere is given by:

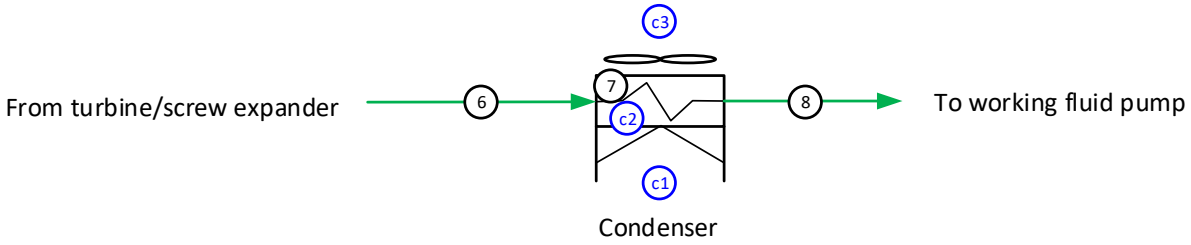

FIGURE 12: Condenser

$$\dot{Q}_{cond} = \dot{Q}_{cond,condenstion} + \dot{Q}_{cond,desuper} \tag{12}$$

$$\dot{Q}_{cond,condenstion} = \dot{m}_{wf} * (h_7 - h_8) \tag{13}$$

$$\dot{Q}_{cond,desuper} = \dot{m}_{wf} * (h_6 - h_7) \tag{14}$$

6.6 Calculation model

A calculation model was made in Engineering Equation Solver (EES) using equations (1) to (14). The model was run for different working fluids and was checked for the best power output using different working fluids like propane, isobutane, isopentane, n-butane and R134a. Excluding propane all the other working fluids showed similar results as shown in the nose diagram in Figure 13.

The model shown in Figure 14 is based on R134a. R134a is the selected working fluid due to its low price, and non-toxicity and non-flammability. Figure 14 shows the calculation model at the best evaporator pressure with thermodynamic stations and outputs. A condensation temperature of 35°C is assumed, which corresponds to roughly 10°C air temperature.

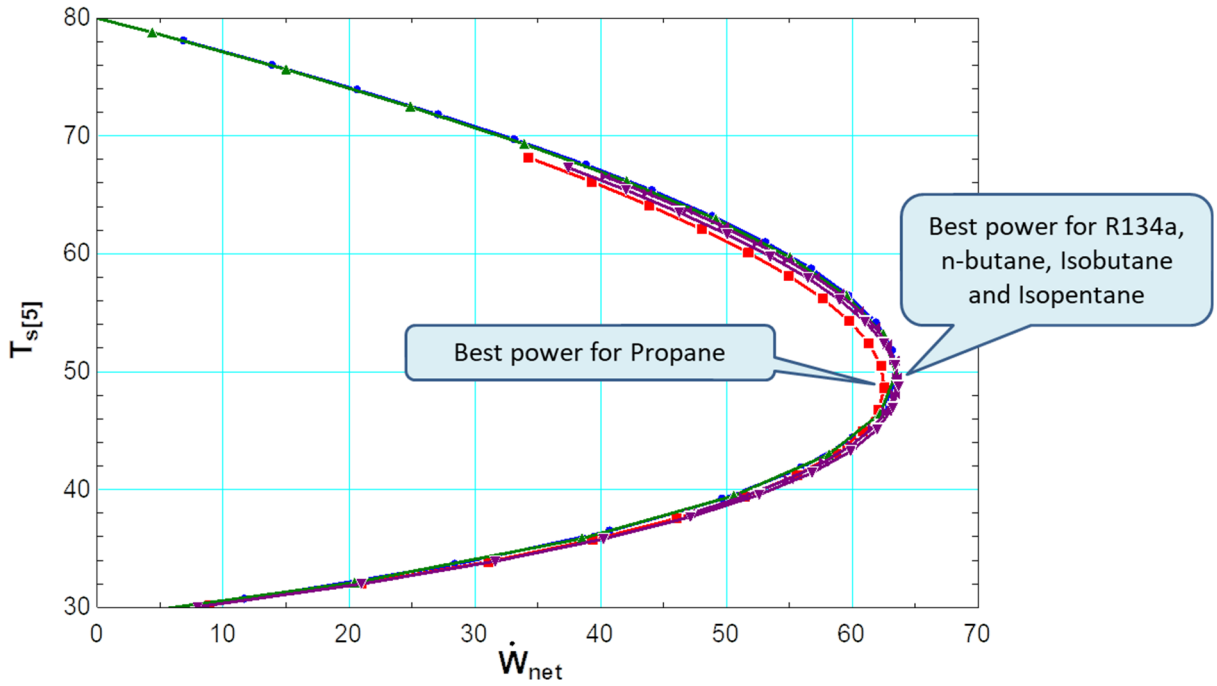

FIGURE 13: Return temperature vs net power output (KW)

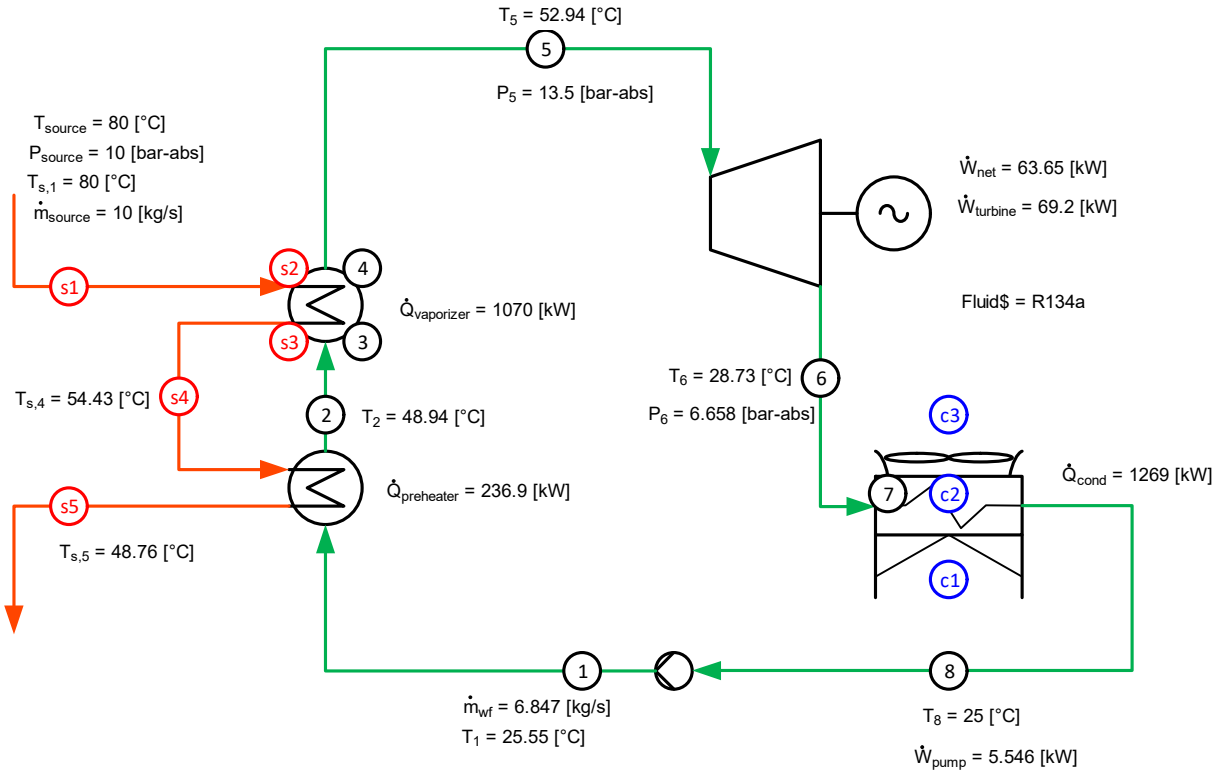

FIGURE 14: Calculation model of the binary power plant

7. HEATING SYSTEM

The temperature in Puga ranges from -25 to 25°C as can be seen from the temperature plot from 2002 to 2011 in Figure 3. Heating is required for almost 7 months a year due to the extreme cold conditions.

7.1 The building to be heated

Nomadic Residential School (NRS) in Puga was started in 2004 by Ladakh Autonomous Hill Development Council (LAHDC), Leh, for the nomadic children of several villages like Korzok, Koyul, Katley, Chumur, Mahey, Samad, Sumdo, Angkung and Kharnak etc. These are the nomads who rear the authentic pashmina for the world. They must move from one place to another for the grazing of their cattle such as yaks and pashmina goats, and therefore their children face difficulty in having a stable education. The NRS is now among the best government schools in the Leh district.

The design conditions of the school building to be heated is given in Table 3.

TABLE 3: NRS in Puga building design condition

Building design conditions	
Latitude	33°13´ N
Elevation	4550 m a.s.l.
Indoor temperature	20°C
Outdoor temperature	-25°C
Name of building	Puga Nomadic Residential School
Distance from the hot spring	1.6 km
Building insulation	None

7.2 The proposed heating system

The proposed heating system will heat the building continuously using the geothermal fluid. The building calculations are based on the building plans shown in Figures 15 and 16.

7.3 Radiator layout

The radiators selected are to be placed underneath the widows and if that is not possible then it should be placed on the external wall side. This is to counteract the cold down draught so as to have comfortable room temperature. The piping is suggested to be put under the ceiling. Such pipe configuration from a temporary building at Keflavik Airport is shown on Figures 17 and 18. Then there is no need to drill holes in the ceiling, and the pipe installation is easy with a minimal inconvenience.

Back pressure in the system is taken care of by a vent in the return line (Figure 19), placed at the highest possible point in the building, above any of the radiators. This ensures higher pressure in the pipeline than the ambient pressure. This is the only way to prevent air leakage into the system and avoid air locks in the radiators without the use of expensive pressure valves.

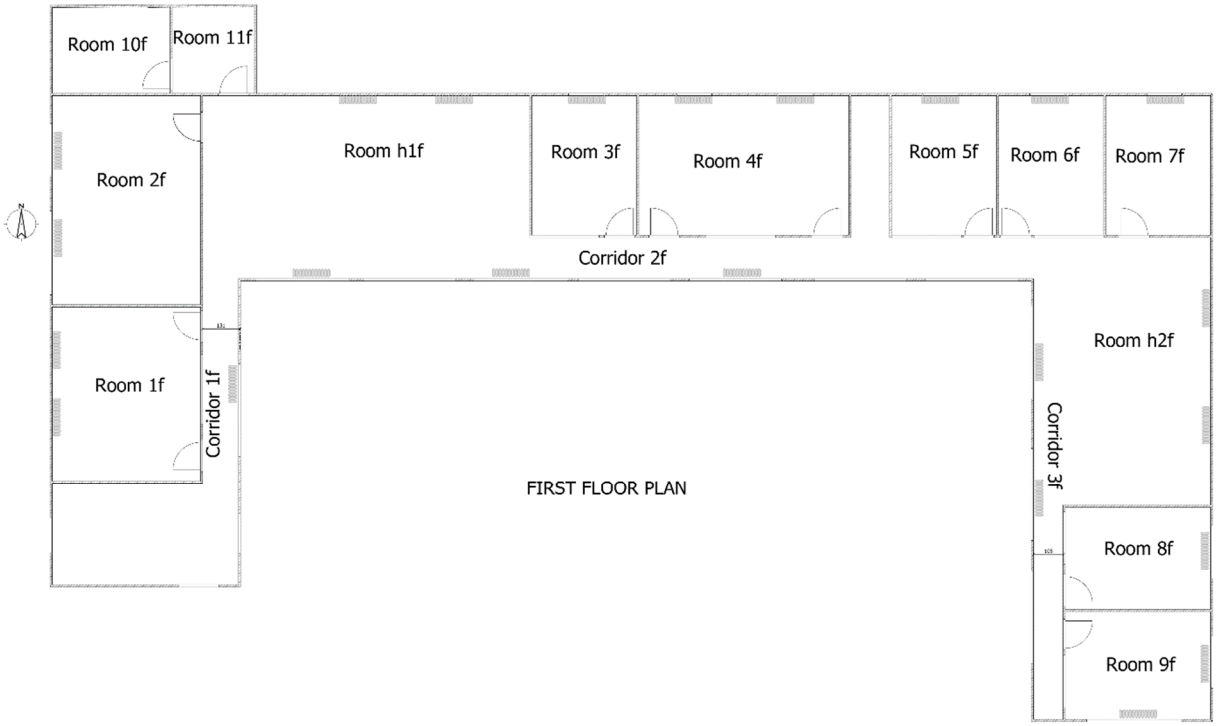

FIGURE 15: First floor plan of Nomadic Residential School, Puga

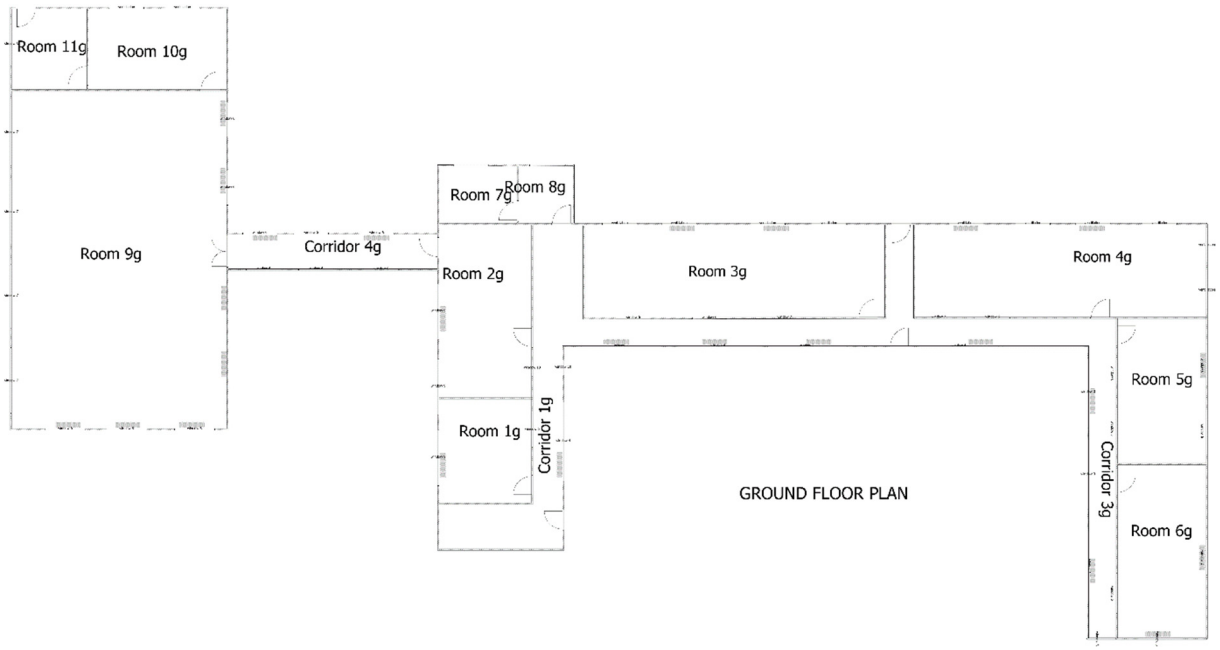

FIGURE 16: Ground floor plan of Nomadic Residential School

FIGURE 17: Pipe layout at Keflavik airport, Iceland

FIGURE 18: Pipe layout at Keflavik airport, Iceland

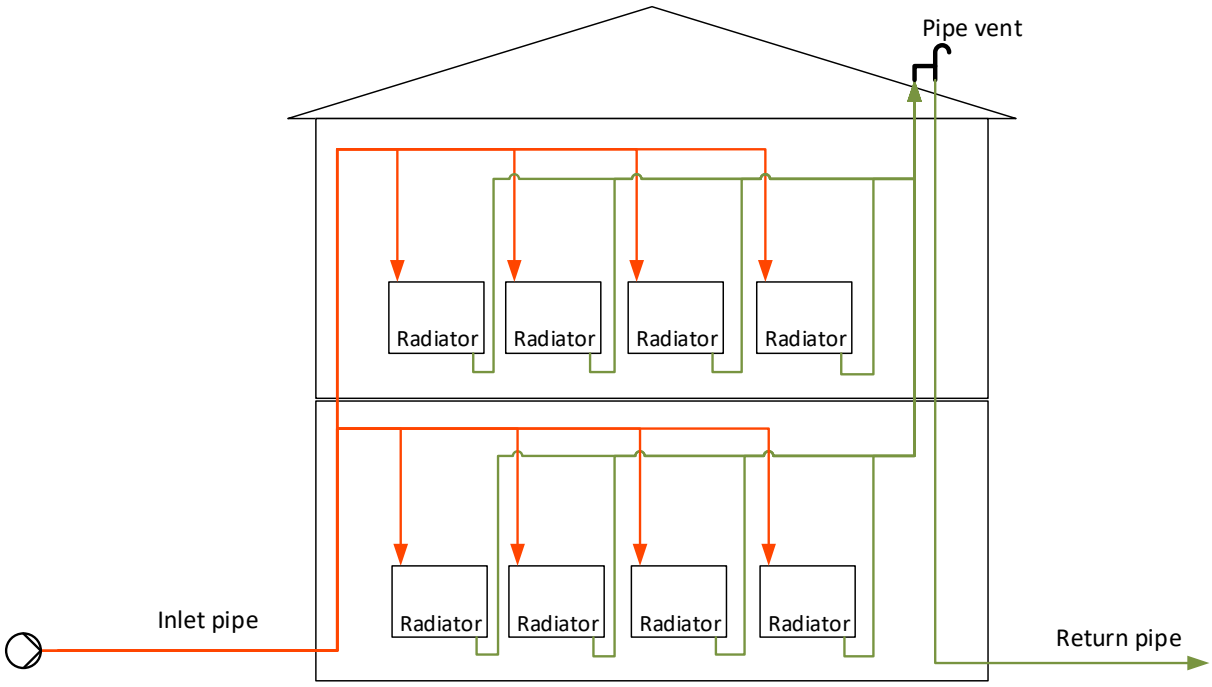

FIGURE 19: Schematic radiator and pipe layout

7.4 Heat load calculation

The purpose of a building's heating, ventilating and air-conditioning system (HVAC) is to maintain a comfort and well-being of the occupants. The procedure followed in the head load calculation is given in Table 4 (Idntaeknistofnun Íslands, 1984).

TABLE 4: Procedure followed in calculation of the heat loss

Procedure
Selection of constant indoor design temperature of 20°C
Selection of outdoor design temperature -20°C
Calculation/selection of the overall heat transfer coefficient, U, for walls, roof, windows, 1 m outer floor, inner floor and doors with the consideration that there is a 15% heat loss due to radiation through the roof
Calculation of the heat load due to transmission and infiltration

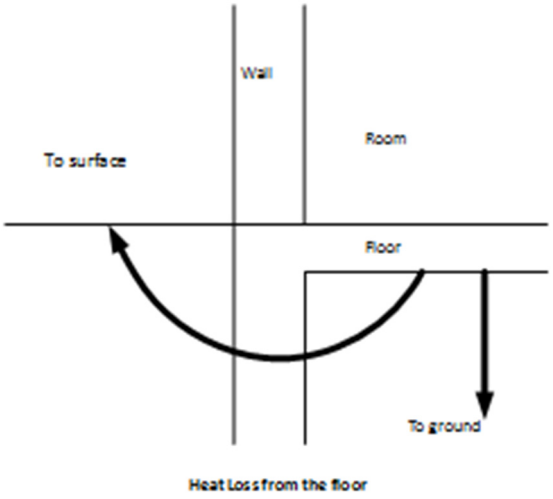

FIGURE 20: Wall layers

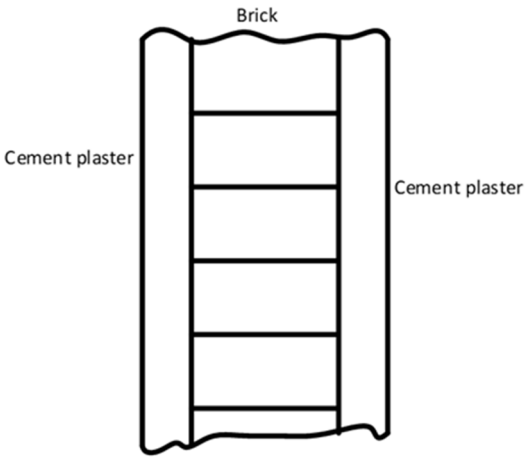

FIGURE 21: Heat loss from floor

7.4.1 Calculation of U values

The building wall is made of mudbrick with cement pilaster as shown in Figure 20. U-values of each component of the building is calculated by considering their individual convection heat transfer coefficients (h), wall conductivity (k) and thickness (dx) of each layer (Idntaeknistofnun Íslands, 1984):

$$\frac{1}{U_{wall}} = \frac{1}{h_{inside}} + \frac{dx}{k_{wall}} + \frac{1}{h_{outside}} \quad (15)$$

$$h_{outside} = \frac{1}{0.13}\frac{m^2°C}{W}$$

The window and ventilation of the building are single pane/glazed with wooden frames and their U values are given as:

$$U_{singlepane} = 7.0\frac{m^2°C}{W}$$

The temperature distribution in the soil under a slab floor changes markedly from season to season (USACERL, 1989). In winter, isotherms are closely bunched near the edge of the floor and heat flux lines are approximate circular arcs from the bottom of the floor to the ground surface (Figure 21). So most heat losses in winter occur at the perimeter. In summer, as the ground warms up, isotherms spread out and are more closely approximate horizontal surfaces and so heat loss is much more uniform over the entire floor. The heat flow resistance values R are taken from (Idntaeknistofnun Íslands, 1984).

$$\frac{1}{U_{outer\ floor}} = R_{soil\ outer} + \frac{dx}{k_{floor}} \quad (16)$$

$$R_{soil\ outer} = 0.7\ \frac{m^2°C}{W}$$

$$\frac{1}{U_{inner\ floor}} = R_{soil\ inner} + \frac{dx}{k_{floor}} \tag{17}$$

The heat flow resistance values R

$$R_{soil\ inner} = 1.5 \frac{m^2°C}{W}$$

The roof of the building is a concrete slab with pilaster on the inner side. Due to radiation there is an additional heat loss from the building to the atmosphere which is estimated to be 15% according to an old Icelandic standard (Idntaeknistofnun Íslands, 1984).

$$\frac{1}{U_{roof}} = \frac{1}{h_{inside}} + \frac{dx}{k_{roof}} + \frac{1}{h_{inside}} \tag{18}$$

The transmissive heat load is given by:

$$Q_{building} = UA_{building} * (T_{inside} - T_{outside}) + UA_{inner\ floor} * (T_{inside} - T_{average}) \tag{19}$$

Heat loss occurs due to infiltration. Infiltration or air leakage (Building Energy Codes, 2011) is the unintentional or accidental introduction of outside air into a building through cracks and use of doors for passage. Whenever there is infiltration there is exfiltration elsewhere in the building which in winter results in movement of warm, moist indoor air towards cold envelope cavities. The heat loss can be calculated as:

$$Q_{infiltration} = n * V_{air,building} *\ \rho * C_{p,air},*\ (T_{inside} - T_{outside}) \tag{20}$$

$$n \geq 0.8\ \left[\frac{1}{hr}\right]$$

In general heat loss from a building is given as

$$Q_{building\ loss} = UA(T_{inside} - T_{outside}) \tag{21}$$

The relative heat load will then be

$$Q_{rel} = \frac{Q_{building\ loss}}{Q_{building\ loss,0}} = \frac{UA(T_i - T_o)}{UA(T_{i,0} - T_{o,0})} \tag{22}$$

where
T_i = inside temperature
T_o = outside air temperature
$T_{i,0}$ = inside temperature at design conditions
$T_{o,0}$ = outside temperature at design conditions

Radiator
In order to determine the size of the radiator, the logarithmic mean temperature difference (LMTD) is found using the following equation

$$\Delta T_m = \frac{(T_s - T_i) - (T_r - T_i)}{\ln \frac{(T_s - T_i)}{(T_r - T_i)}} \tag{23}$$

LMTD at design conditions is given by

$$\Delta T_{m,0} = \frac{\left(T_{s,0} - T_{i,0}\right) - \left(T_{r,0} - T_{i,0}\right)}{\ln\left(\frac{T_{s,0} - T_{i,0}}{T_{r,0} - T_{i,0}}\right)} \tag{24}$$

Relative heat load of radiator is given by

$$Q_{rel} = \frac{Q}{Q_0} = \left(\frac{\Delta T_m}{\Delta T_{m,0}}\right)^{\frac{4}{3}} \tag{25}$$

where Q_{rel} = relative heat load of radiator
Q =actual heat output from the radiator
Q_0 =heat output of radiator at design conditions

Water/geothermal fluid heat duty
Relative heat load of water flow is

$$Q_{rel} = \frac{Q_{water}}{Q_{water,0}} \tag{26}$$

$$Q_{rel} = \frac{\dot{m} \cdot C_p \cdot (T_s - T_r)}{\dot{m}_0 \cdot C_p \cdot \left(T_{s,0} - T_{r,0}\right)} \tag{27}$$

where Q_0 = heat load due to hot water passing through the radiator
$Q_{water,0}$ = heat load due to hot water passing through radiator at design conditions.

Pipe calculation
The pressure head loss due to friction in the pipeline from the geothermal source to the building inlet is determined by the Darcy-Weisbach equation. It is considered the best empirical relation for pipe flow resistance (Biosystems, 2017).

$$H_L = \frac{f \cdot L \cdot \bar{v}^2}{d \cdot 2 \cdot g} \tag{28}$$

where
f = friction factor
L = Length of pipe from the geothermal source to the building inlet
$\bar{v}$ = average fluid velocity
Head losses due to sudden changes in the flow are given by the following equation:

$$H_L = K\frac{v^2}{2 \cdot g} \tag{29}$$

where
K = loss coefficient for the type of bends

7.4.2 ASRAHE heat load calculation method

The heat load calculations follows the method given by ASRAHE, 2009, except a more simple treatment was used for the ground floor heat loss. There the Old Icelandic Standard is used (Idntaeknistofnun Íslands, 1984), dividing the ground floor into inner and outer sections. The outer section is calculated in the same way as in the ASRAHE method, calculating the heat flow to the surrounding air and adding soil heat resistance. The inner section is calculated in a simpler way by assuming a soil resistance and that the heat transfer is to the undisturbed ground, having the same temperature as the average yearly air temperature. The outer section is taken as a 1 metre wide band of the floor from the outer building wall.

7.4.3 Simplification based on Icelandic standard ÍST 66

The Icelandic standard has been used for the heat load calculation in this report. U values were calculated for the building components like the doors, windows, walls, 1 metre outer floor, inner floor, and roof. It is important to account for heat transfer from the inner floor area of a medium to large building. The temperature distribution in the soil under a slab floor changes markedly from season to season (USACERL, 1989). In winter, isotherms are closely bunched near the edge of the floor and heat flux lines approximate circular arcs from the bottom of the floor to the ground surface. So, most heat losses in winter occurs at the perimeter. In summer, as the ground warms up isotherms spread out and more closely approximate horizontal surfaces and so heat loss is much more uniform over the entire floor.

7.5 Radiator selection

Radiators were selected from Maktek (2017), on the basis of the results given in Table 7. Here type 33 radiators are selected so as to reduce the area occupied by them. There will be only one main valve to control the flow in the radiators. Individual valves on the radiators are avoided to as to save on cost.

7.6 Benefits of improved building insulation

Calculation was also done considering that the building is insulated with 0.05 m thick extruded polystyrene (thermocol) insulation (U=0.033) and double-glazed windows. It was found that the heat load reduced to 36 percent as can be seen in Table 7. These conditions can be considered in the future to reduce the heating requirement of the building. The potential savings (Dickson and Fanelli, 2003) can also be seen in Table 5.

TABLE 5: Effect of insulation on building heating demand

Insulation criteria	Typical heating demand (kWh/year)	Glazing type
Insignificant insulation	>100000	Single
Poor insulation	55300	Single
Icelandic building code	30000	Double
Swedish building code	26800	Triple
Super insulation	22500	Quadruple

7.7 Calculation model

Calculation was done for the various components of the building as shown in Table 6.

TABLE 6: U value for building components

Item	Area (m^2)	U value without insulation (W/m^2)	U value with insulation (W/m^2)
Net effective outside wall	769.4	1.44	0.45
Windows	256.7	7.0	3.5
Door	48.51	0.64	0.64
Outer floor section on ground floor	263.6	0.6	0.31
Inner floor section on ground floor	375.8	1.15	0.42
Roof of first floor	390.7	2.5	0.52

8. SYSTEM SIMULATION

8.1 Duration curves

The duration curves are estimated form the IWEC weather data for Shiquanhe (ASHRAE, 2017). Shiquanhe (4255 m a.s.l.), is the main town of Ngari district in China which lies on same altitude as Puga. The town of Shiquanhe is shown in Figure 22. This data is on an hourly basis, and describes what is considered to be a typical year. The data is reduced to 14 points, which was deemed to be sufficiently accurate to make the duration curves.

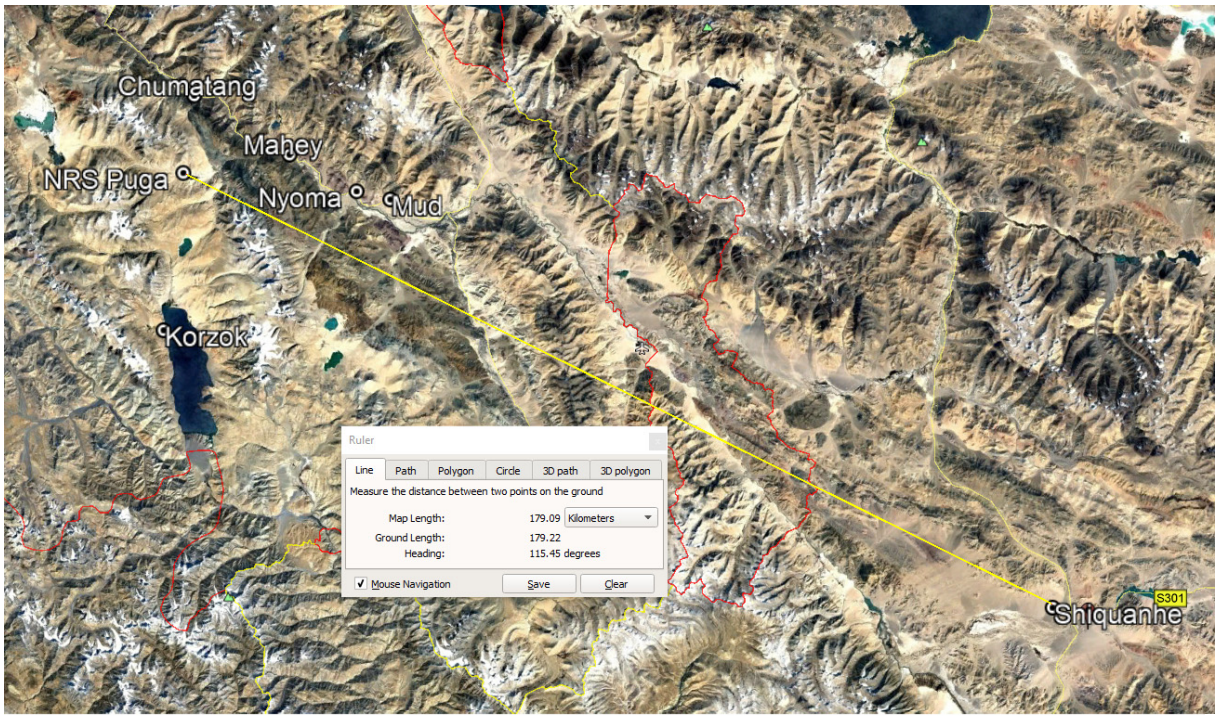

FIGURE 22: Map showing distance between Puga, India and Shiquanhe town of Ngari district, China

The duration curve for the outdoor air temperature for Shiquanhe is shown in Figure 23.

The heat load for the duration curves is calculated from a slightly simplified heat load calculation method. There it is assumed that all heat is lost to the ambient air, and the heat transfer coefficient for the building is obtained from the heat load which was calculated as reference (design) heat load.

$$U_{building} = \frac{\dot{Q}_{reference}}{(T_{indoor} - T_{outdoor,reference})} \tag{30}$$

The heat load for any outdoor temperature is then calculated from:

$$\dot{Q}_{building} = U_{building} \cdot (T_{indoor} - T_{outdoor}) \tag{31}$$

8.2 Heat load for individual rooms

Table 7 gives the heat load for the building and the radiator model selected on the basis of heat load of building without insulation which is the present case.

TABLE 7: Heat load and radiator selected

Heat loss for each rooms	With insulation	Without insulation	Radiator model	No of radiator	Length
Room 1g	2050	4870	33-PKKPKP 900	1	3.00
Room 2g	2317	5456	33-PKKPKP 900	1	3.00
Room 3g	3748	9262	33-PKKPKP 600	2	3.00
Room 4g	3554	9156	33-PKKPKP 600	2	3.00
Room 5g	2327	5378	33-PKKPKP 900	1	3.00
Room 6g	2500	6542	33-PKKPKP 600	2	2.00
Room 9g	11443	38145	33-PKKPKP 900	7	3.00
Room 10g (kitchen)	1884	6304	0.00	0	0.00
Corridor 4g	3650	7704	33-PKKPKP 900	2	2.00
Corridor ground floor	10194	21910	33-PKKPKP 600	7	2.00
Room 1f	1798	6070	33-PKKPKP 600	2	2.00
Room 2f	2035	6704	33-PKKPKP 600	2	2.00
Room 3f	1139	3536	33-PKKPKP 900	1	2.00
Room h1f	1636	7080	33-PKKPKP 900	2	2.00
Room 4f	1908	6355	33-PKKPKP 600	2	2.00
Room 5f	1139	3536	33-PKKPKP 900	1	2.00
Room 6f	1139	3536	33-PKKPKP 900	1	2.00
Room 7f	839	3061	33-PKKPKP 600	1	2.00
Room 8f	1238	3718	33-PKKPKP 900	1	2.00
Room h2f	1373	5964	33-PKKPKP 600	2	2.00
Room 9f	2342	6122	33-PKKPKP 600	2	2.00
Corridor first floor	13644	32947	33-PKKPKP 900	6	3.00
Total heat loss	**73899**	**203357**			

The duration curve for the building heat load is shown on Figure 24. There is heat load for almost the whole year, there are only roughly 120 hours every year with an air temperature above 20°C.

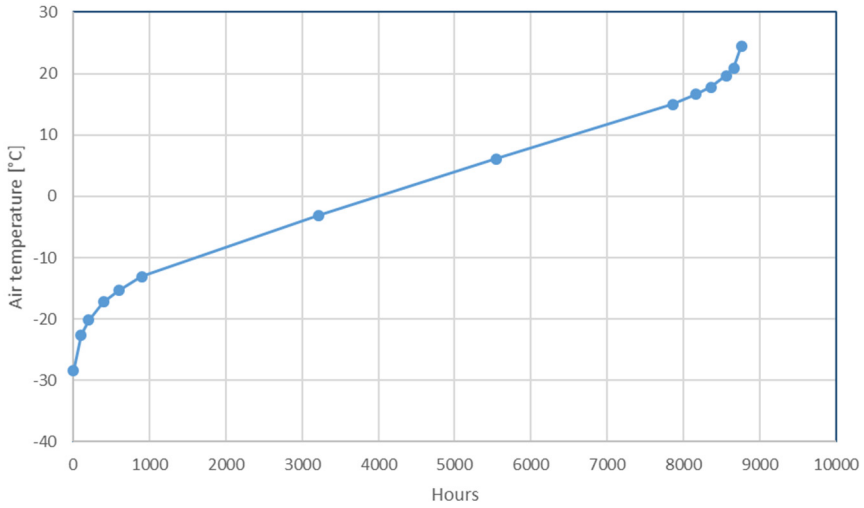

FIGURE 23: Duration curve of the outdoor air temperature

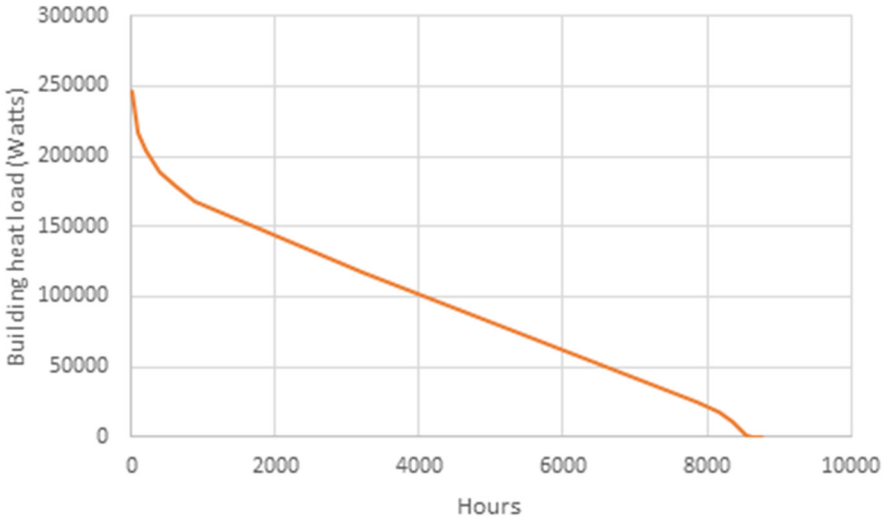

FIGURE 24: Heat load of building vs hours

8.3 Pipe transmission effectiveness

The geothermal fluid will lose some heat before reaching the building. This heat loss can be expressed by use of the "transmission effectiveness" which is defined in Valdimarsson (1993). Transmission effectiveness, τ, is the ratio of the temperature drop of the transmitted water to the temperature difference between the system inlet temperature and the ground temperature. In cases where the outlet water temperature equals the ground temperature, τ is 0. τ is 1 if there is no temperature drop through the transmission. The transmission effectiveness at design condition, τ_0, is used to determine the distribution system quality. The transmission effectiveness is given as

$$\tau = \tau_0 \frac{\dot{m}_0}{\dot{m}} \tag{32}$$

The supply temperature to the building inlet is calculated by

$$T_{s,building} = T_{ground} + (T_{s,geothermal} - T_{ground}) \cdot \tau \tag{33}$$

where

$T_{s,building}$ = Supply temperature at building inlet
T_{ground} = Temperature of ground
$T_{s,geothermal}$ = Temperature of geothermal source

The duration curve of the transmission effectiveness is shown on Figure 25. The transmission effectiveness proves to be higher than 60% for roughly 8300 hours every year. That means that there will be an "acceptable" supply temperature at the building for at least 8300 hours per year. Rest of the time is when the air temperature is so high that there is low water flow to the building, and heating is almost not needed.

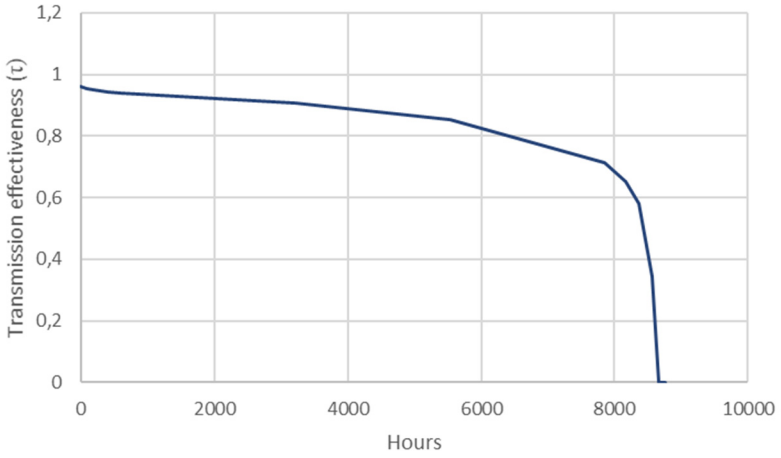

FIGURE 25: Pipe transmission effectiveness

The duration curve for the water supply temperature at the building is shown on Figure 26.

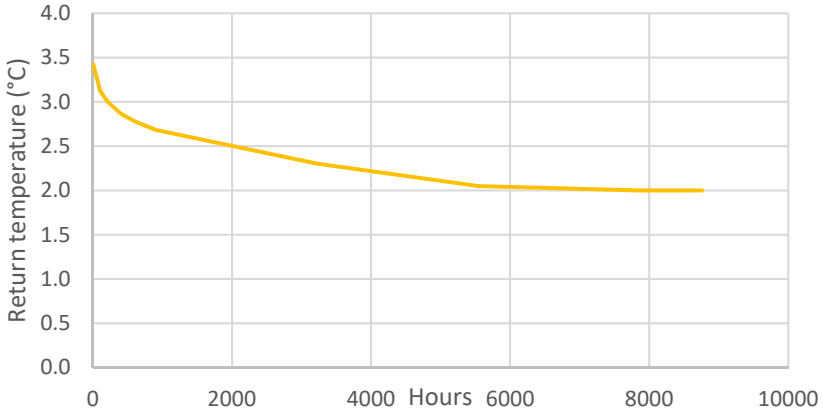

FIGURE 26: Building supply temperature vs hours a year

If higher water temperature is required due to some reason, then a bypass will have to be made at the school to increase flow in the supply pipe and thereby reduce the temperature loss in the pipe. The bypass flow would then have to be disposed of at the school site. The duration curve for the geothermal water mass flow is then calculated (Figure 27). There is no tap water consumption, so the flow goes to zero when the air temperature is at or above 20°C.

The radiator return temperature is now calculated and the duration curve is shown on Figure 28. The return temperature approaches the indoor temperature of 20°C when the heat load is low. Then the flow though the radiators is very low and the water cools down to the indoor temperature in the radiator.

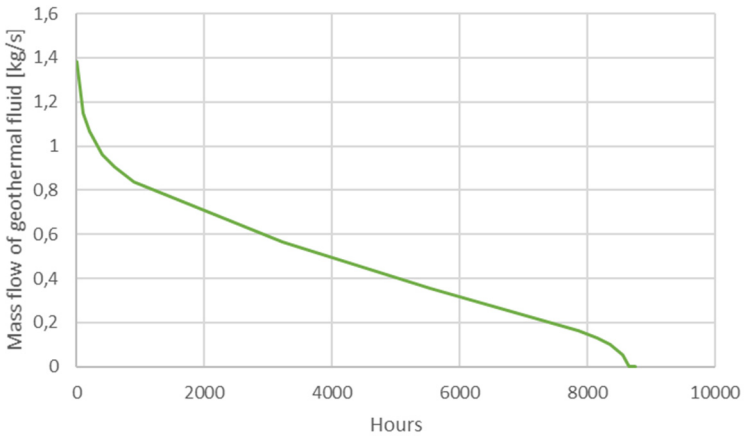

FIGURE 27: Mass flow of geothermal fluid vs hours

9. COST ESTIMATION

The tentative cost estimation given in Table 8 is made on the basis of prevailing prices in Iceland. Prices for the pipes and bends are from Set ehf. a pipe company in Selfoss and Bauhaus building market in Reykjavik. Radiator prices are from Maktek Company, Turkey. Transportation cost and taxes are not considered here.

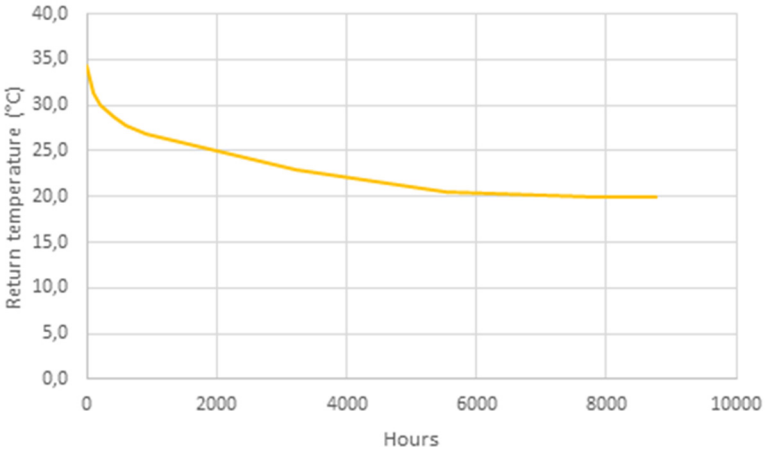

FIGURE 28: Return temperature of building vs hours

TABLE 8: Tentative cost of co-generation

Items	Unit cost [USD/m, USD/ea]	No. of units/length	Total cost (USD)
Steel pipe pre-insulated for district heating	20/m	1600 m	32000
Trenching cost	20/m	1600 m	32000
Piping within the building, alupex or calpex	6/m	720 m	4320
Cost of radiators			7000
Cost of radiator temperature control valve	50/pc	49 nos	2450
Bends, nipples etc for piping (4 for each radiator)	15/pc	196 nos	2940
Cost for power plant	2500/kW	70 kW	175000
Administrative cost (5% of the total project cost)			12786
Total main component cost			**268596**

10. CONCLUSIONS AND RECOMMENDATIONS

The available geothermal source can be utilised to provide continuous electricity and heating for the boarding school. The utilisation will make the building sustainable in that it will not have to depend on fossil fuels which are used at present to electrify and heat the building. These fossil fuels are now transported from the main town of Leh which is 176 km away. At present the building has no insulation due to which there is a large heat load. For the long term benefit and energy savings the building should be insulated, which will reduce the heating load by more than half compared to the present.

The implementation of this project will bring a change in the lives of the students living there. They will have electricity 24 hour per day which will be truly beneficial and make a significant difference in their lives. They will not have to gather wood and use kerosene for heating to keep them warm in the cold winter months. They will be able to enjoy living in a clean environment with this sustainable energy solution. Living in high altitudes can be very challenging in many aspects so any efforts in making the lives of people more comfortable and adaptable is worth the effort.

Estimated geothermal potential of India is 10,600 MWe from more than 300 sites with more than 20 hot springs in the state of Jammu and Kashmir (Craig et al., 2013). Chumathang and Puga in the Indus valley and Panamik in Nubra valley are said to have geothermal potential between 3 and 20 MWe. Deep drilling of more than 2000 metres will provide geothermal fluid with temperature of above 200°C. As a start, a binary power plant of 20 MW capacity can be set up in this field which can act as a base load for Leh district which can run continually unlike the hydroelectric power plants which run under capacity especially in winters. The geothermal potential of the region needs to be utilised in order to have a sustainable source of energy rather than using fossil fuels.

ACKNOWLEDGEMENTS

I would like to thank Jigmet Takpa, IFS, (Ex Project Director, Ladakh Renewable Energy Development Agency) Joint Secretary, Ministry of Environment Forest and Climate Change, Government of India, for giving me the opportunity to undertake this course. Thanks to my supervisor, Dr. Páll Valdimarsson for your effort and sharing your experiences.

Many thanks goes to Lúdvík S. Georgsson, Ingimar Gudni Haraldsson, Málfrídur Ómarsdóttir, Thórhildur Ísberg and Markús A.G. Wilde for organising the training and getting us taught by the best in the industry, making sure everything went well from the course lectures to our stay and field trips. Thanks to all the staff from Orkustofnun, ISOR, Iceland University, Reykjavik University and other various fields and organisations. My special thanks to Stella for always keeping the lunch ready on time.

Thanks to funding agency United Nations and Iceland University. Thanks to all the staff at Indian Embassy in Iceland which was a home away from home. Thanks to my family, relatives and friends back home for their constant support. My special thanks to Juliet Newson, Director, Iceland School of Energy and Dr Ahsan Absar for their valuable suggestions and guidance.

Thank you all UNU Fellows of 2017, and MSc and PhD Fellows from so many countries. Thanks to my roommates, El Fina and Li Yiman for surviving together without any catfights. Exergy group, you were the best.

Lastly thanks to my daughters, Kunsal and Kundon whose love kept me strong.

REFERENCES

ASHRAE, 2009: *Residential cooling and heating load calculations.* ASHRAE Handbook – Fundamentals, Chapter 17, 16 pp.

ASHRAE, 2017: International weather files for energy calculations 2.0 (IWEC2). ASHRAE research project RP-1477, “Development of 3012 typical year weather files for international locations" carried out by White Box Technologies, Moraga, Ca, with principal investigator Huang, Y.J., website: *www.ashrae.org/resources--publications/bookstore/iwec2.*

Azeez, K.K.A., and T., Harinarayana, 2007: Magnetotelluric evidence of potential geothermal resource in Puga, Ladakh, NW Himalaya. *Current Geoscience, 93*, 323-329.

Biosystems, 2017: The Darcy-Weisbach equation. In: *Henry Darcy and his law*. Biosystems, Oklahoma State University, website:
www.biosystems.okstate.edu/faculty-sites/Darcy/DarcyWeisbach/Darcy-WeisbachEq.htm

Building Energy Codes, 2011: *Building technologies program, air leakage guide.* US DoE, Energy Efficiency and Renewable Energy, Sept., 38 pp.

Craig, J., Absar, A., Bhat, J., Cadel, G., Hafiz, M., Hakhoo, N., Kashkari, R., Moore, J., Ricchiuto, T.E., Thuro, J., and Thusu, B., 2013: Hot springs and the geothermal potential of Jammu and Kashmir State, NW Himalaya, India. *India´s Earth Science Reviews, 126,* 156-177.

Dickson, H.M., and Fanelli, M, 2003: *Geothermal energy utilization and technology*, *space and district heating.* UNESCO Publishing, France, 221 pp.

District Statistical and Evaluation Office, 2015: *Statistical handbook 2014-15 for Leh district.* Government of Jammu and Kashmir, Leh Planning and Development Department, Ladakh Autonomous Hill Development Council*,* 231 pp.

Elíasson, E.T., Thórhallsson, S., and Steingrímsson, B., 2008: Geothermal Power Plants. *Proceedings of Short Course on Geothermal Project Management and Development, organised by UNU-GTP, KenGen and MEMD-DGSM, at the Imperial Botanical Beach Hotel, Entebbe, Uganda,* 15 pp.

Harinarayana, T. Azzez, K.K.A., Naganjaneyulu, C., Manoj, C., Veeraswamy, D.N., Murthy, S., Rao., S.P.E., 2004: Magnetotelluric studies in Puga geothermal field, NW Himalaya, India. *Journal of Volcanology and Geothermal Research, 138*, 405-424.

Idntaeknistofnun Íslands, 1984: *Icelandic standard IST 66* (in Icelandic). UDC 699.86, 57-81 pp.

Maktek., 2017: *Panel radiator*. Maktek, Turkey, website: *maktek.com.tr/en/radyator-2/.*

Shanker, R., Absar, A., Srivastava, G.C., and Bajpai, I.P, 2000: *A case study of Puga geothermal system, Ladakh, India.* Geological Survey of India, Luknow, India, 7 pp.

Singh S.B., Drolia, R.K., Sharma, S.R., and Gupta, M.L., 1983: Application of resistivity surveying to geothermal exploration in the Puga Valley, India. *Geoexploration, 21-1*, 1-11.

United Nations, 2015: *Sustainable Development Goals – 17 Goals to transform our world*. UN, website: *www.un.org/sustainabledevelopment/sustainable-development-goals/*

USACERL, 1989: *Three dimensional modelling of heat transfer from slab floors.* US Army Corps of Engineers Construction Engineering Research Laboratory, Technical Manuscript E-89/11, 213 pp.

Valdimarsson, P., 1993: *Modelling of geothermal district heating systems*. University of Iceland, Ph.D. thesis, 315 pp.

Yue-feng, Y.U., Da, H.U., and Fang-zhi, W.U., 2015: Applications of the screw expander in geothermal power generation in China. *Proceedings of the World Geothermal Congress 2015 Melbourne, Australia,* 7 pp.